Journal of Materials Chemistry A

ROYAL SOCIETY OF CHEMISTRY

PERSPECTIVE

View Article Online
View Journal

Cite this: DOI: 10.1039/d5ta06105a

Decoding pH-dependent electrocatalysis through electric field models and microkinetic volcanoes

Songbo Ye,[ab] Yuhang Wang,[a] Heng Liu,[a] Di Zhang,[a] Xue Jia,[a] Linda Zhang,[ac] Yizhou Zhang,[a] Akichika Kumatani,[abde] Hitoshi Shiku *[b] and Hao Li *[a]

The impact of electrolyte pH on electrocatalytic reactions has long been recognized, yet its underlying mechanisms remain a subject of active debate. This perspective explores how pH influences reaction activity and mechanisms at the computationally affordable atomic scale. Traditional interpretations attribute pH effects to changes described by the computational hydrogen electrode (CHE) model and the Nernst equation. However, recent advances have uncovered more complex interfacial interactions involving electric fields, including dipole moments (μ), polarizability (α), and the potential of zero charge (PZC). We summarize recent progress on how pH influences surface states and reaction mechanisms across various typical electrocatalytic processes, including the hydrogen evolution reaction (HER), oxygen reduction reaction (ORR), carbon dioxide reduction reaction (CO_2RR), and nitrate reduction reaction (NO_3RR). By integrating experimental observations with theoretical models and computational simulations, researchers are beginning to unravel the multifaceted role of pH in electrocatalysis. Furthermore, several key theoretical frameworks have been developed to date to predict reaction activity and elucidate underlying mechanisms, such as the reversible hydrogen electrode (RHE)-referenced Pourbaix diagram and the pH-dependent microkinetic volcano model. Understanding these pH-driven effects is essential for designing catalysts that operate efficiently across diverse electrochemical environments, ultimately contributing to the development of sustainable energy technologies.

Received 29th July 2025
Accepted 10th September 2025

DOI: 10.1039/d5ta06105a

rsc.li/materials-a

1. Introduction

Electrocatalysis plays a central role in clean energy conversion technologies, including water splitting, CO_2 reduction, ammonia synthesis, *etc.*[1–5] A fundamental challenge in understanding and designing efficient electrocatalysts lies in accurately modeling the electrochemical interface under realistic operating conditions.[6] Among these, pH emerges as a critical environmental variable,[7] influencing reaction thermodynamics,[8] kinetics,[9] surface states (*i.e.*, the electrochemistry-induced surface coverage and reconstruction),[10] *etc.* However, capturing pH-dependent behavior remains nontrivial due to the complex coupling between proton transfer, interfacial electric fields, and the stability of realistic adsorbates.[11–14] Conventional approaches, such as the seminal computational hydrogen electrode (CHE) model, relate Gibbs free energies to the reversible hydrogen electrode (RHE) potential and include pH effects *via* the Nernst equation.[15] However, this treatment assumes idealized conditions and often neglects both the implicit and explicit roles of pH in modulating electric fields, realistic surface states, and proton donors, *etc.*[16,17] When simulating pH effects using explicit solvation with hundreds of water molecules and including cations and/or anions, the dynamic nature of the water structure can introduce significant fluctuations and deviations.[18–20] To mitigate this, it is necessary to average the results over a significant number of distinct explicit solvent configurations under *ab initio* molecular dynamics (AIMD) simulations.[21] However, this approach requires substantial computational resources. A thorough understanding of how pH influences electrocatalytic reactions requires theoretical models that go beyond simple thermodynamics, and meanwhile, maintaining the required computational cost at an affordable level. Recently, researchers have proposed theoretical models that incorporate electric field effects, such as RHE-level surface Pourbaix diagram and pH-dependent volcano, overcoming the partial limitations of the traditional CHE model.[1,22] It also exhibits a similar scope of application.

[a]*Advanced Institute for Materials Research (WPI-AIMR), Tohoku University, Sendai 980-8577, Japan. E-mail: li.hao.b8@tohoku.ac.jp*

[b]*Graduate School of Engineering, Tohoku University, 6-6-11 Aramaki-aza Aoba, Aoba-ku, Sendai 980-8579, Japan. E-mail: hitoshi.shiku.c3@tohoku.ac.jp*

[c]*Frontier Research Institute for Interdisciplinary Sciences, Tohoku University, Sendai 980-0845, Japan*

[d]*Department of Electrical and Electronic Engineering, Chiba Institute of Technology, Chiba 275-0016, Japan*

[e]*Precursory Research for Embryonic Science and Technology, Japan Science and Technology Agency (JST), Saitama 332-0012, Japan*

First, a key issue lies in establishing models for pH-dependent surface states. Previous models mostly relied on the CHE model to construct surface Pourbaix diagrams.[23–25] This approach simplifies the influence of pH, which sometimes leads to significant discrepancies between theoretical predictions and experimental observations. For example, during HER in acidic media, experiments have suggested that the Pt(111) surface is precovered by H*,[26] whereas under the same RHE-scale potential in alkaline media, the surface could be largely precovered by HO*.[2,27] However, the classic surface Pourbaix diagram predicts H* coverage as dominant under HER conditions across acidic, neutral, and alkaline media.[28,29] By incorporating electric field effects, an innovative RHE-level surface Pourbaix diagram has been proposed, reproducing the HO*-covered surface state of Pt(111) in alkaline environments.[10] Moreover, in alkaline environments, the actual surface coverages of adsorbed species (*e.g.*, H* and HO*) significantly influence HER activity. High coverage of HO* can block active sites and inhibit proton/electron transfer, rendering the desorption of HO* the rate-determining step (RDS) of the reaction.[2]

Catalytic volcano models are widely used as both conceptual and quantitative tools to predict the activity trends of electrocatalysts by using key thermodynamic descriptors, such as the binding energy of intermediates.[8,29–31] Traditionally, these volcano plots are constructed under standard conditions without explicitly considering the influence of environmental variables such as pH. However, pH can significantly alter both the thermodynamics and kinetics of electrochemical reactions.[32] By incorporating pH-dependent parameters into the descriptor-based framework, modified pH-dependent volcano plots can be constructed that reflect how catalytic activity varies across different pH regimes. For example, on Au(111) and Au(100) surfaces, the formation of HOO* serves as the RDS, and their adsorbate binding energies exhibit strong dependence on the electric field. This leads to significantly enhanced ORR activity under alkaline conditions (where a more negative electric field is present).[16] Furthermore, Zhang *et al.*[21] derived a pH-dependent ORR volcano model to identify the "acid trap" issue in metal–nitrogen–carbon (M–N–C) single-atom catalysts (SACs), with excellent agreement with experimental observations – this further illustrates that pH can even break the conventionally known Sabatier principle.

Another noteworthy issue is the change in proton donors, which can significantly affect the reaction mechanism and energy barriers.[33,34] Especially for HER, the electric field may indirectly modulate the reaction by affecting OH adsorption or water molecule orientation, but the intrinsic energy barrier difference between proton donors (H_3O^+ *vs.* H_2O) is the primary cause of the pH effect.[17,35–37] By considering the differences in reaction energy barriers between different proton donors, Liu *et al.*[9] simulated polarization curves that closely match experimental results,[4] further revealing that the sluggish kinetics of alkaline HER mainly originate from the increased energy barrier of the water dissociation step (*i.e.*, the Volmer step).

To systematically analyze the pH dependence in electrocatalytic processes, this perspective is organized as follows: (1) we first provide a comparative analysis of electric field models currently used to investigate pH effects, elaborating on the fundamental principles and computational workflows. (2) We then discuss how to theoretically analyze the realistic surface states of electrocatalysts under specific pH conditions, emphasizing the critical role of this step in understanding the structure–activity relationship of materials. (3) Furthermore, we present the methodologies for constructing pH-dependent volcano plots and evaluate their reliability and applicability in predicting the catalytic performance of hydrogen evolution reaction (HER), oxygen reduction reaction (ORR), carbon dioxide reduction reaction (CO_2RR), and nitrate reduction reaction (NO_3RR) across different pH environments. Through these discussions, we aim to provide methodological guidance and a conceptual framework for incorporating pH effects into future theoretical studies of electrocatalyst design.

2. Models for exploring the effects of pH

To simulate the effect of pH, conventional models often adopt the CHE approach and introduce the pH dependence of the RHE to simplify the treatment.[8] In electrochemical studies, the CHE method serves as one of the most important theoretical reference frameworks, establishing the relationship between the standard hydrogen electrode (SHE) and the RHE. Under standard conditions, the relationship between RHE and SHE is given by: USHE = URHE − 0.0591 × pH. This expression is derived from the Nernst equation and reflects the influence of pH on the electrode potential (Fig. 1a). Based on this model, the effect of pH on catalytic thermodynamics can be simplified. In the past, most theoretical surface state analyses were based on the conventional CHE model to construct surface Pourbaix diagrams, aiming to predict the realistic surface states of electrocatalysts under reaction conditions.[24] Building upon this framework, researchers further employed surface-state-informed models to calculate key activity descriptors, such as the adsorption energies of reaction intermediates, and combined these with traditional volcano plots to enable rapid screening of catalytic performance. Under alkaline ORR conditions (*e.g.*, pH = 13, at 0.8 V/RHE), ZrN(100) is predicted to be covered by 1 ML HO*, as confirmed by the classic 2D Pourbaix diagram. Electric field simulations show that this coverage reduces the dipole moment and polarizability of O*, enhancing ORR activity by facilitating O–O bond activation. The adsorption energy calculated based on the HO*-covered model successfully predicted the high activity of the surface, in agreement with experimental observations.[38] Furthermore, according to the classic 1D Pourbaix diagram, Wang *et al.*[39] recently revealed that the high NRR activity of FeS_2 catalysts originates from the *in situ* formation of sulfur vacancies during electrochemical operation. DFT calculations showed that under NRR-relevant conditions, S-vacancy-decorated FeS_2(111) is thermodynamically favored. These vacancies enhance N_2 adsorption and modify the catalytic pathway, successfully explaining the experimentally observed performance.

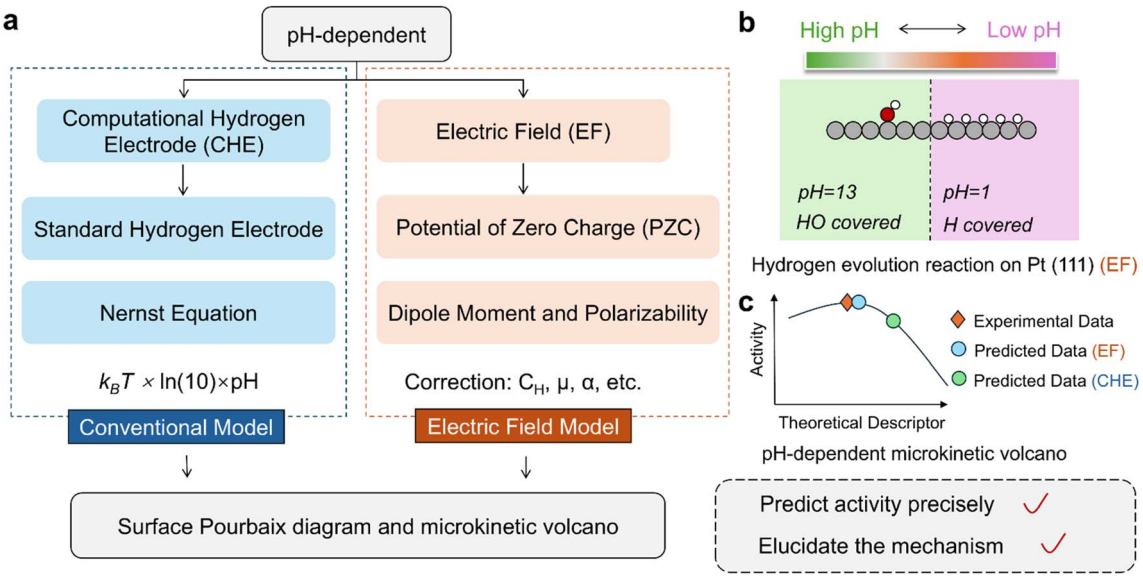

Fig. 1 Schematic illustrations of: (a) the methods dealing with pH for the classic CHE model and the electric field (EF) pH-dependent model; (b) surface coverage on Pt(111) revealed by the electric field model: HO* dominates under alkaline conditions, while H* prevails under acidic conditions; (c) simplified pH-dependent activity volcano.

However, this conventional method only introduces pH corrections on a thermodynamic scale and often neglects deeper effects of pH on interfacial electric fields, proton donor change, and pH-dependent surface state. As a result, it presents certain limitations when applied to complex systems. The electric field model demonstrates improved accuracy in simulating pH-dependent surface states and catalytic activities. Each adsorbate's dipole moment (μ) and polarizability (α) were extracted by fitting a second-order polynomial to energy-field data, using $G_{ads} = G_{ads}^{PZC} + \mu\vec{E} - \frac{\alpha}{2}\vec{E}^2$, where G_{ads}^{PZC} refers to the binding energy of adsorbate at the potential of zero charge (PZC).[16,40,41] For example, in acidic and alkaline media, the Pt(111) surface tends to be covered by different species, H* in acid and HO* in base,[2,27] yet this pH-dependent surface state cannot be explained by classical surface Pourbaix diagrams based on the CHE model. In contrast, models that incorporate electric field effects offer more accurate predictions of pH-dependent activity and better capture the influence of interfacial environments on surface coverage (Fig. 1b and c).[10] Furthermore, the electric field model also plays an important role in elucidating reaction mechanisms. IrO_2 is one of the mostly used catalysts under acidic conditions for the OER, yet its reaction mechanism remains debated. DFT calculations combined with microkinetic modeling reveal that the polarization of reaction intermediates significantly affects the potential response, potentially leading to misinterpretation of the mechanism. By incorporating electric field effects, researchers successfully reproduce the experimental Tafel curves.[42]

To more clearly illustrate the advantages of the electric field model over conventional approaches—such as the CHE modeling capturing pH-dependent behavior, we presented pH-dependent schematic free energy diagrams (Fig. 2a) and corresponding microkinetic volcano (Fig. 2b) that incorporate interfacial electric field effects. As shown in Fig. 2a, under a fixed U_{RHE}, CHE model typically yields static free energy diagrams, wherein the reaction barriers remain unchanged across different pH conditions. However, when the electric field model is employed to account for interfacial field effects, the reaction free energy landscape becomes pH-dependent, even at constant U_{RHE}.[42] This demonstrates the advanced capability in capturing subtle but crucial pH-induced changes that are otherwise overlooked. Further, this will lead to microkinetic volcanoes exhibiting pH dependence (Fig. 2b).[16] More importantly, as shown in Fig. 3c, the impact of the interfacial electric field is species-specific (different intermediates respond differently to the field). Most adsorbates show modest dipole moments, causing slight destabilization under increasing electric fields. In contrast, $H_2O_2^*$ and HOO* possess large polarizabilities, resulting in significant stabilization at both positive and negative fields, mainly due to their geometry changes in response to the field. The O_2^* intermediate exhibits a higher electric field sensitivity than O*. Due to the different electric field responses of various adsorbate species, the RDS may be changed. This challenges the previously established mechanistic intuitions, offering a more dynamic and realistic framework for analyzing electrocatalytic reaction pathways. For example, in ORR on Au(100), the 2e-processes are limited by producing *OOH when in acid. In base, however, *OOH is stabilized so much that it is no longer limited in the 2e-process. Instead, the 2e-process becomes limited by production of $*H_2O_2$ from *OOH. Subsequently, more accurate pH-dependent polarization curves and Tafel plots on the Au(100) were simulated.

To construct accurate pH-dependent electrocatalysis models, benchmarking against experimental results is a critical step.

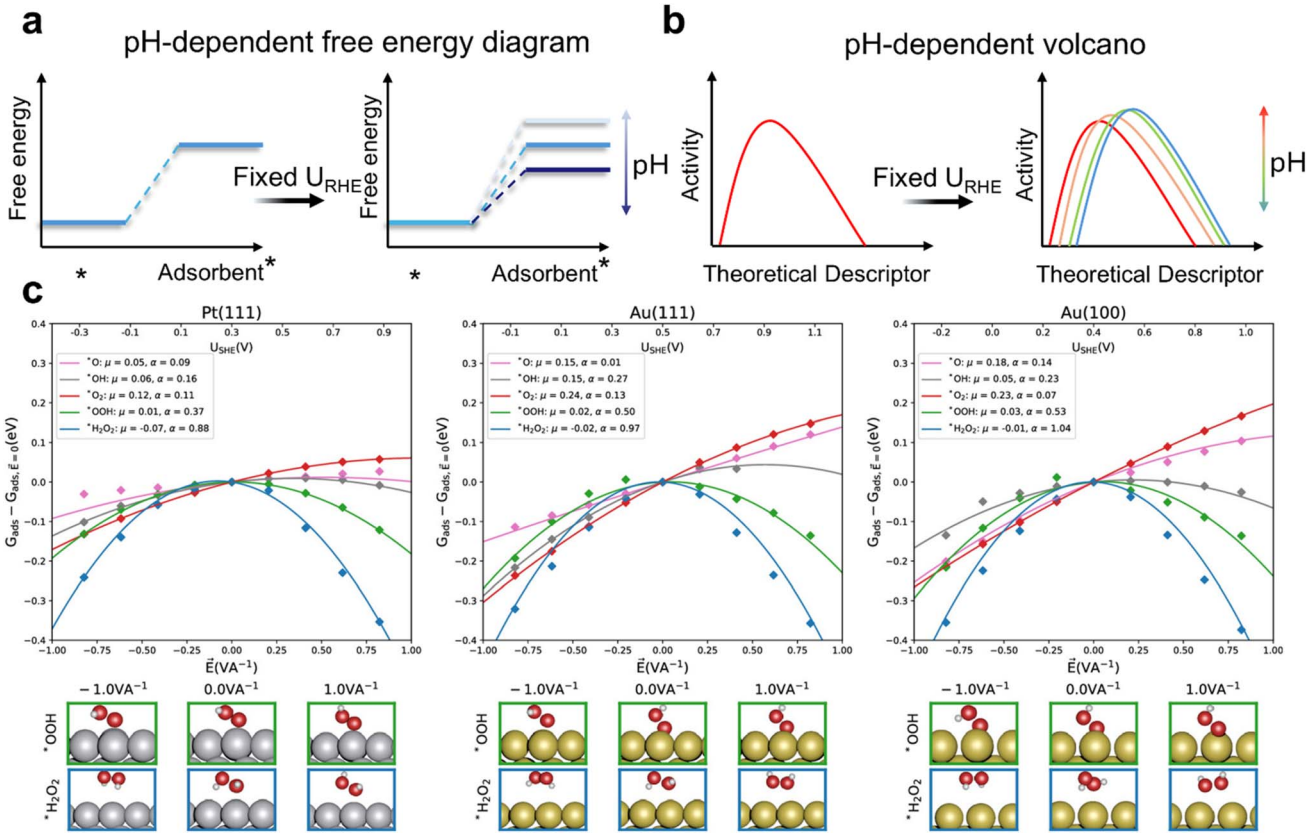

Fig. 2 Schematic illustrations of: (a) pH-dependent free energy diagram and (b) pH-dependent volcano at a fixed U_{RHE}. (c) Electric field effects on ORR adsorbates with fitted values for μ (e) and α (e^2 V^{-1}) for Pt(111), Au(111), and Au(100). Reproduced with permission.[16] Copyright 2020, American Chemical Society.

Previous studies have typically selected catalyst systems with well-characterized structures and validated the reliability and applicability of theoretical predictions, such as surface states and reaction trends, through integration with *in situ* experimental observations.[43–46] With the advancement of large language models and materials databases (Fig. 3a), AI-assisted high-throughput exploration of pH effects on catalytic activity is emerging as a new research paradigm.[47–50] Researchers are increasingly leveraging data-driven approaches to identify pH-dependent trends while integrating accurate theoretical models to interpret experimental observations. This synergy between data-driven discovery and mechanistic understanding is paving the way for a more systematic and intelligent development of electrocatalysis. Zhang *et al.*[21,51] proposed that M–N–C catalysts exhibit significant differences under varying pH conditions (Fig. 3b). Some Fe-centered SACs show weak pH dependence, with Fe-pyrrole-N_4 demonstrating better ORR performance than Fe-pyridine-N_4 in acidic media. Co-centered catalysts display higher H_2O_2 selectivity under acidic conditions, while pyrolysis-prepared catalysts generally have lower faradaic efficiency compared to molecular catalysts.[52] Some M–N–C SACs show low pH sensitivity and 4e$^-$ ORR selectivity comparable to noble metals in both acidic and alkaline media, whereas others exhibit high pH sensitivity and elevated H_2O_2 selectivity, resembling transition metal compounds.[53] They also identified the "acid trap" issue through their modeling, which is in excellent agreement with the subsequent experimental validations. These differences provide important guidance for catalyst design. Wang *et al.*[54] suggest that, based on a large-scale data mining analysis of the experimental CO_2RR performance of 2348 reported catalysts, the violin plot of formic acid (HCOOH) faradaic efficiencies (Fig. 3c) for Sn-based catalysts reveals that both selectivity and activity increase with rising pH, as exemplified by SnO_2 and $Bi_{0.1}Sn$.[55,56] They further developed a pH-dependent model to explain the reaction mechanism.

When constructing computational models, it is crucial to first account for the explicit effects of pH on catalytic reactions, such as pH-dependent surface states and pH-dependent reaction mechanisms that lead to variations in reaction barriers (Fig. 3d–g). McCrum *et al.*[2] suggest that alkaline HER activity correlates with the HO* adsorption strength, successfully explaining the experimentally observed volcano curve. Then they identified, in the 2D volcano plot, the region where HO* desorption is the RDS. However, in the classical surface Pourbaix diagram, the Pt(111) surface is predicted to be covered by H* across the entire pH range (Fig. 3d). By incorporating electric field effects into the model, a pH-dependent surface state model was developed that simulates the surface being covered by HO*

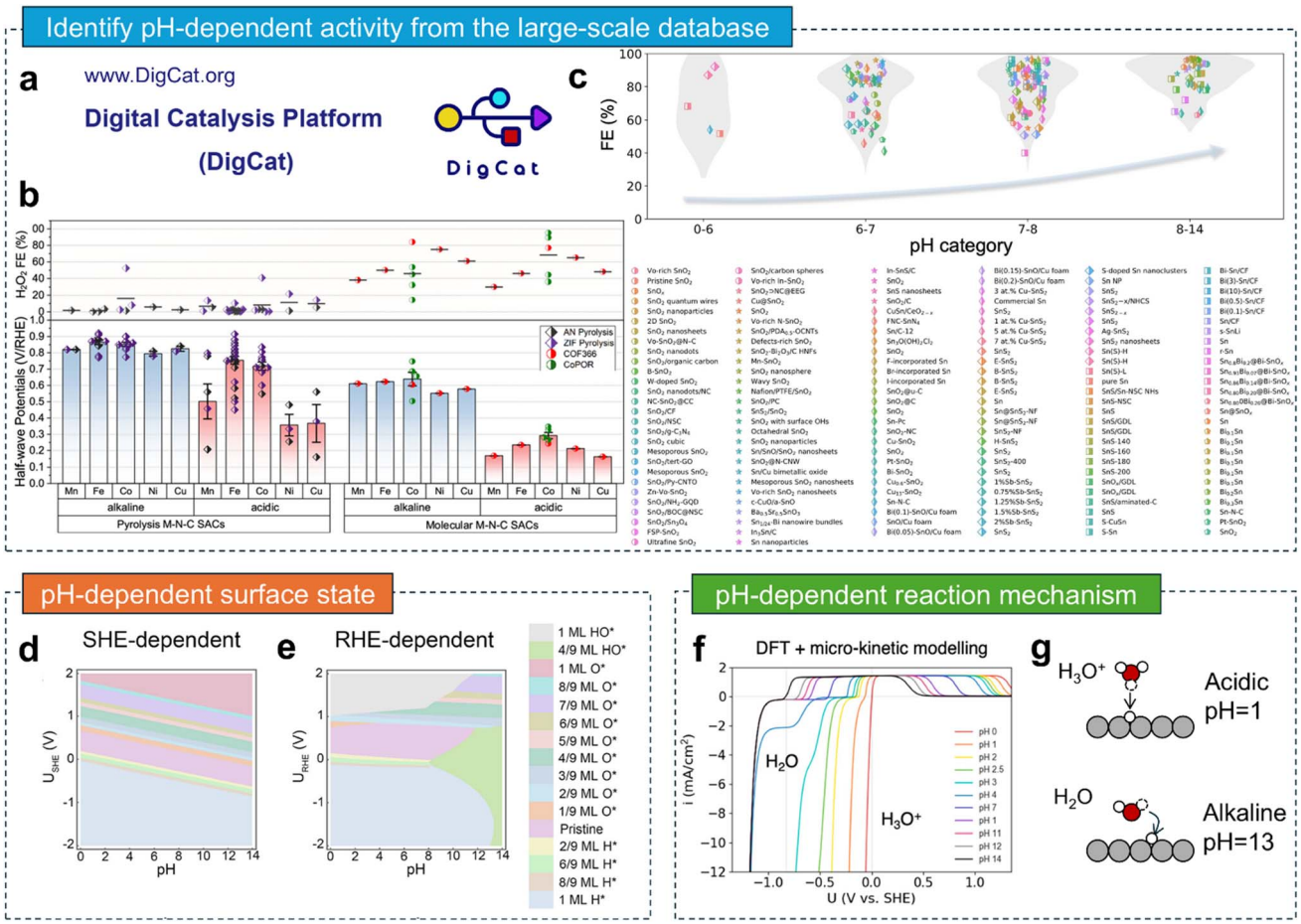

Fig. 3 Discovering the correlation between pH and catalytic activity through large-scale database: (a) a representative large-scale experimental database, the Digital Catalysis Platform (DigCat: https://www.digcat.org);[49] (b) ORR activity analysis of >100 reported M–N–C catalysts. Data points were extracted from the original references based on the following conditions: the half-wave potential is the potential at which the current reaches half the value of the diffusion limiting current, and the faradaic efficiency (FE%) is calculated at 0.6 V *vs.* RHE; Reproduced with permission.[21] Copyright 2024, American Chemical Society. (c) Summary of the experimental CO_2RR performance of 2348 reported catalysts *via* a large-scale data mining. Violin plot of Sn-based catalysts for formic acid (HCOOH) formation under different reduction environments, ranging from acidic to alkaline conditions. Reproduced with permission.[54] Copyright 2024, Wiley-VCH. The pH-dependent surface states of Pt(111): (d) the SHE-dependent surface Pourbaix diagram based on classical CHE method, and (e) the RHE-dependent surface Pourbaix diagram based on the electric field model. Reproduced with permission.[10] Copyright 2024, American Chemical Society. pH-dependent reaction mechanism of HER: (f) simulated polarization curves using the DFT-activation energies and mean-field microkinetic modeling, and (g) Volmer step of the HER in acidic and alkaline conditions. Reproduced with permission.[17] Copyright 2019, American Chemical Society.

under neutral and alkaline conditions (Fig. 3e), which agrees with experimental observations. Furthermore, as the pH shifts from acidic to alkaline conditions, the proton donor in the HER may change from H_3O^+ to H_2O. Using HER models developed for acidic conditions to predict HER activity in alkaline media can severely underestimate the reaction energy barriers, leading to misleading conclusions. Lamoureux *et al.*[17] investigated the influence of shifts in hydrogen binding, proton donor, and water reorganization energy. They suggest that the intrinsically larger barriers for the splitting of water with respect to hydronium are the cause of HER kinetics being slower in alkaline than in acidic media. By considering this change, they simulated the polarization curves using the DFT activation energies and mean-field microkinetic modeling, which explains the experimental observation (Fig. 3f and g).[4,57–59]

3. pH-dependent electrocatalytic surfaces

To gain a comprehensive understanding of the realistic catalytic surface under varying pH conditions, especially in complex environments, it is necessary to consider the effects of the electric field. For each adsorbate, the binding energies were corrected by applying the electric field effects at the given U_{RHE}. This approach calculates the dependence of the binding energy on pH by incorporating experimentally measured values of the PZC and the Helmholtz capacitance (C_H). By doing so, the method accounts for the influence of the interfacial electric field on adsorption energetics, providing a more accurate and realistic description of the electrochemical interface. Fig. 4a–c

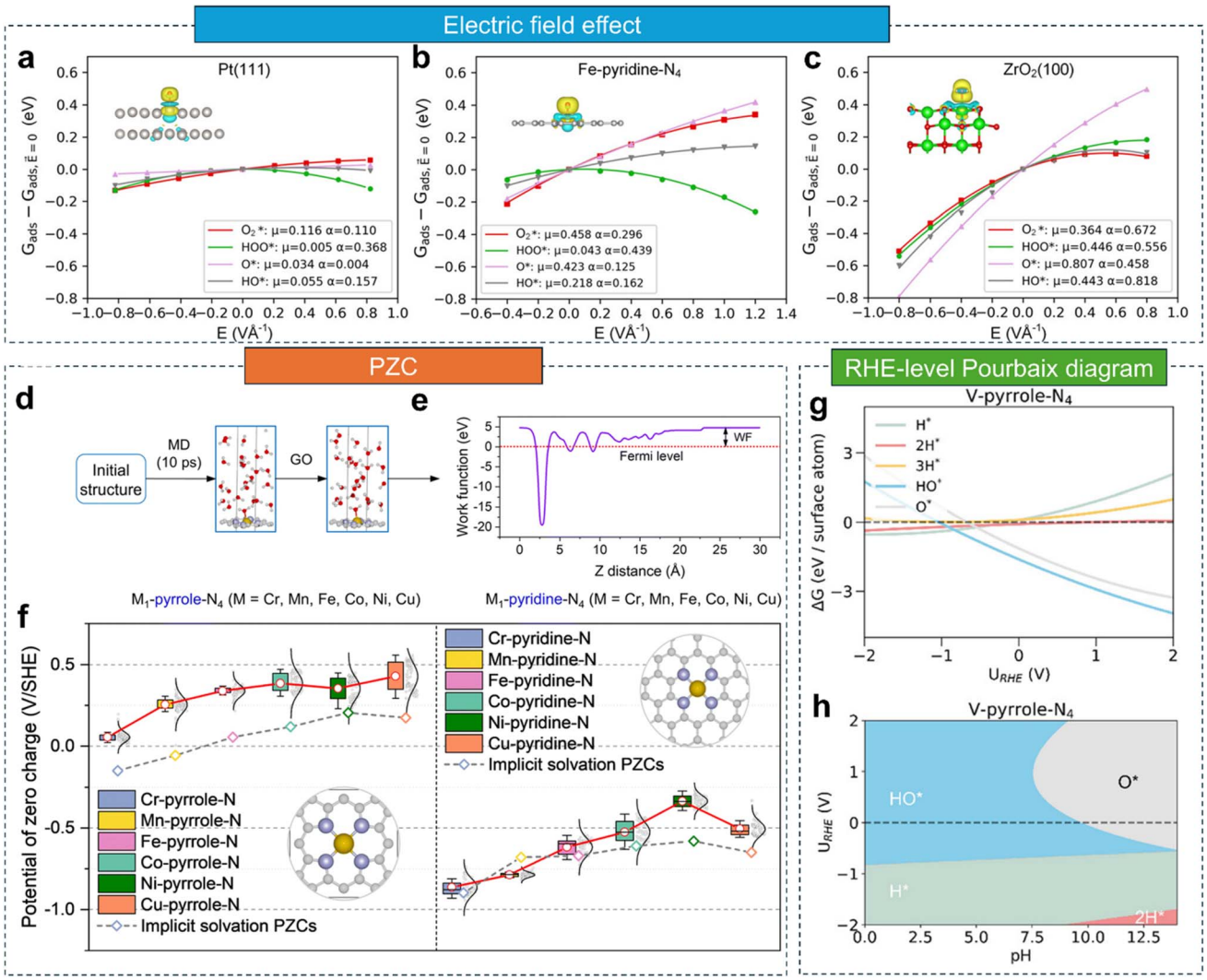

Fig. 4 (a–c) Electric field effects on the adsorption free energies of ORR adsorbates. Reproduced with permission.[21] Copyright 2024, American Chemical Society. Determination of the PZCs in M–N–C catalysts using an explicit solvation model: (d) illustration of the PZC calculation workflow; (e) the work function (WF) of materials in ion-free water is utilized to calculate PZC; (f) PZCs of the two typical M–N–C configurations: M-pyrrole-N_4 and M-pyridine-N_4. Reproduced with permission.[67] Copyright 2024, Royal Society of Chemistry. (g) Calculated 1D surface Pourbaix diagram and (h) pH- and RHE-dependent 2D surface Pourbaix diagrams. Reproduced with permission.[22] Copyright 2025, Wiley-VCH.

show how ORR adsorbates respond to varying electric fields on transition metals (TMs), M–N–C catalysts, and transition metal compounds (TMXs). M–N–C catalysts exhibit moderate sensitivity to electric field changes, especially for adsorbed O*, falling between the responses of TMs and TMXs. Different adsorbates respond differently to electric fields, which means the surface state might change when considering this crucial factor.[42]

Electrochemical interfacial properties, such as the PZC and the structure of the electric double layer (EDL) at the electrode–electrolyte interface, are of great importance for understanding the activity and selectivity of electrocatalysts. In theories, Fig. 4d shows the workflow of acquiring the PZC values on the M–N–C configurations. For each M–N–C structure, 10 000 structures were sampled *via* AIMD over 10 ps. 100 typical configurations were then selected and relaxed. PZCs were then calculated as work functions under explicit solvation, referenced to the absolute potential of the SHE (Fig. 4e).[21] Fig. 4f shows that differences in N-coordination structures lead to variations in the calculated PZC values, incorporating both explicit and implicit solvation models. This seems to explain the differences in alkaline HER activity of M–N–C with different N coordination.[60] More importantly, there is a linear relationship between the HO* binding energy descriptor and the PZC, which supports incorporating the effect of PZC while using the binding energy as a single descriptor. Similarly, this method can be applied to metal and alloyed metal surfaces (including terrace and step geometries) and predict the PZC based solely on the HO* binding energy and the vacuum work function estimated from static DFT calculations.[61] In experiments, Kim *et al.*[62] first measured the PZC on Pt thin-film electrodes using scanning electrochemical cell microscopy (SECCM), and then conducted HER activity tests on eight selected regions of bare Pt and Pt–Pd–Ru–Ir–Ag surfaces. The results showed that the high-entropy alloys with higher PZC components exhibited higher HER

activity.[62] These results emphasized the PZC influences during both experimental and theoretical process. After considering the linear relationship between HO* binding energies, H* binding energies, and PZC as well as the electric field effects, Ye *et al.*[22] applied 1D/2D RHE-level surface Pourbaix diagrams in SACs design. This work explained why catalysts with optimized H* binding energy exhibit poor HER activity (*e.g.*, V-pyrrole-N_4) and proposed a 2D HER microkinetic model combining both H* binding energies and HO* binding energies to address the main controversies currently existing in SACs HER studies. Combining the results of Fig. 4g and h, the poisoning of active sites by HO*/O* has become the main factor limiting HER activity of V-pyrrole-N_4.[63–66]

4. Revisiting catalytic microkinetic volcano plots through the lens of pH

Catalytic volcano plots are a typical theoretical model for correlating catalytic activity with the binding energy of key reaction intermediates (*e.g.*, H* for HER and HO* for ORR).[68–72] They reflect the Sabatier principle: catalysts that bind intermediates too strongly or too weakly show poor performance, while those with optimal binding energies lie near the volcano peak and exhibit the highest activity.[73–75] This approach helps explain activity trends and guides the rational design of electrocatalysts. However, most previous volcano models have simplified or overlooked the influence of pH, which is crucial yet challenging to accurately capture based on conventional CHE models. In addition, these models are generally based on thermodynamics and do not consider kinetic factors such as coverage and kinetic barriers. These pose significant challenges in accurately elucidating the true reaction mechanisms and properly accounting for the influence of pH.

Herein, we summarize several recent typical studies that incorporate pH effects (*i.e.*, the electric field model) into microkinetic volcano models, aiming to provide theoretical guidance and insights for the design of pH-dependent catalytic reactions, including ORR, CO_2RR, HER, and NO_3RR. We systematically summarized these models in terms of how they account for the influence of pH, reaction mechanisms, and other key factors.

Currently, microkinetic models obtain the reaction rates of a series of elementary steps by solving a mean-field microkinetic model at steady state.[76–78] An important step of this model is identifying scaling relationships between different reaction species and kinetic barriers. Tang *et al.*[69] calculated the scaling relations of the charge extrapolated Volmer, Heyrovsky, and Tafel transition state energies *vs.* H* binding energy, then derived the HER microkinetic volcano (Fig. 5a). The HER exchange current densities of several metals were calculated, which are in good agreement with experimental results. Using this model, a plateau region was identified in the volcano plot dominated by the Volmer–Tafel mechanism, which support the Volmer–Heyrovsky mechanism. This also provided insights that later enabled successful prediction of the HER activity of 2D transition-metal dichalcogenides.[70] Similarly, the scaling relationship between HO* and HOO* binding energies control the OER/ORR activities, which in most cases follows the equation $\Delta E_{OOH} = \Delta E_{OH} + 3.2$ eV (Fig. 5b). It should be noted that this scaling relationship is suitable for many types of catalysts, such as metals, metal oxides, and M–N–C SACs, *etc.*[1,21] In contrast, the scaling relationship between HO* and O* binding energies is more site/catalyst-specific (Fig. 5c). Subsequently, the pH effect (*via* the electric field model) was integrated into the microkinetic modeling framework, enabling the construction of a pH-dependent microkinetic volcano model (Fig. 5d–g):

- ORR: Li *et al.*[21] used the electric field model combined with an ORR microkinetic model to reveal that the generally lower ORR activity of transition metal oxides (TMOs) compared to Pt is mainly due to weak oxygen binding energy and strong electric field effects that hinder O–O bond cleavage. They also found that TMOs perform better under alkaline conditions, while the electric field effect significantly reduces their activity in acidic environments, consistent with experimental observations. Based on the scaling relationships and electric field model of M–N–C SACs, the pH-dependent ORR TOF value matched well with the experimental results and revealed the "acid trap" issue (Fig. 5d).[21] Kelly *et al.*[16] investigated ORR microkinetic volcano models for $2e^-$ and $4e^-$ ORR and revealed that pH dependence arises from electric field effects, which impact catalysts differently based on their adsorption strengths. On Au(100), negative fields strongly enhance ORR activity by stabilizing O_2* and HOO*, while Pt(111) shows minimal change. This leads to similar activity for Au(100) and Pt(111) in base.[79] Experimental currents at 0.9 V/U_{RHE} match the model predictions that consider field effects, highlighting their predictive power. Au surfaces show strong field sensitivity, especially for O_2^* and HOO*, making them more active in alkaline media.

- CO_2RR: Fig. 5e simulates the formation rate (TOF) of HCOOH under varying *OCHO binding energies and electric field conditions (corresponding to pH). The results show that for the Sn–N_4–C single-atom catalyst, the volcano plot shifts to the right under alkaline conditions, indicating enhanced activity. In contrast, for polyatomic Sn catalysts, the volcano shifts to the left as pH increases. This difference arises from opposite changes in dipole moment and polarizability upon *OCHO adsorption, induced by structural differences. Further analysis reveals that the rate-determining step varies with pH for the two types of catalysts, leading to opposite trends in activity. Therefore, the model highlights the structural sensitivity of Sn-based catalysts to pH: enhancing *OCHO adsorption can improve activity for SACs, while weakening it is more favorable for polyatomic Sn – different catalysts design should be adopted accordingly. The theoretical current density curves under different pH conditions show good agreement with the experimental data; despite slight deviations, the overall consistency is high. Furthermore, machine learning potentials accelerate molecular dynamics simulations, while pH-field coupled microkinetic modeling reveals pH-dependent CO_2RR behavior on the RHE scale. SnO_2 nanorod formation and SnS_2 surface roughening were accurately captured, consistent with experiments.[80]

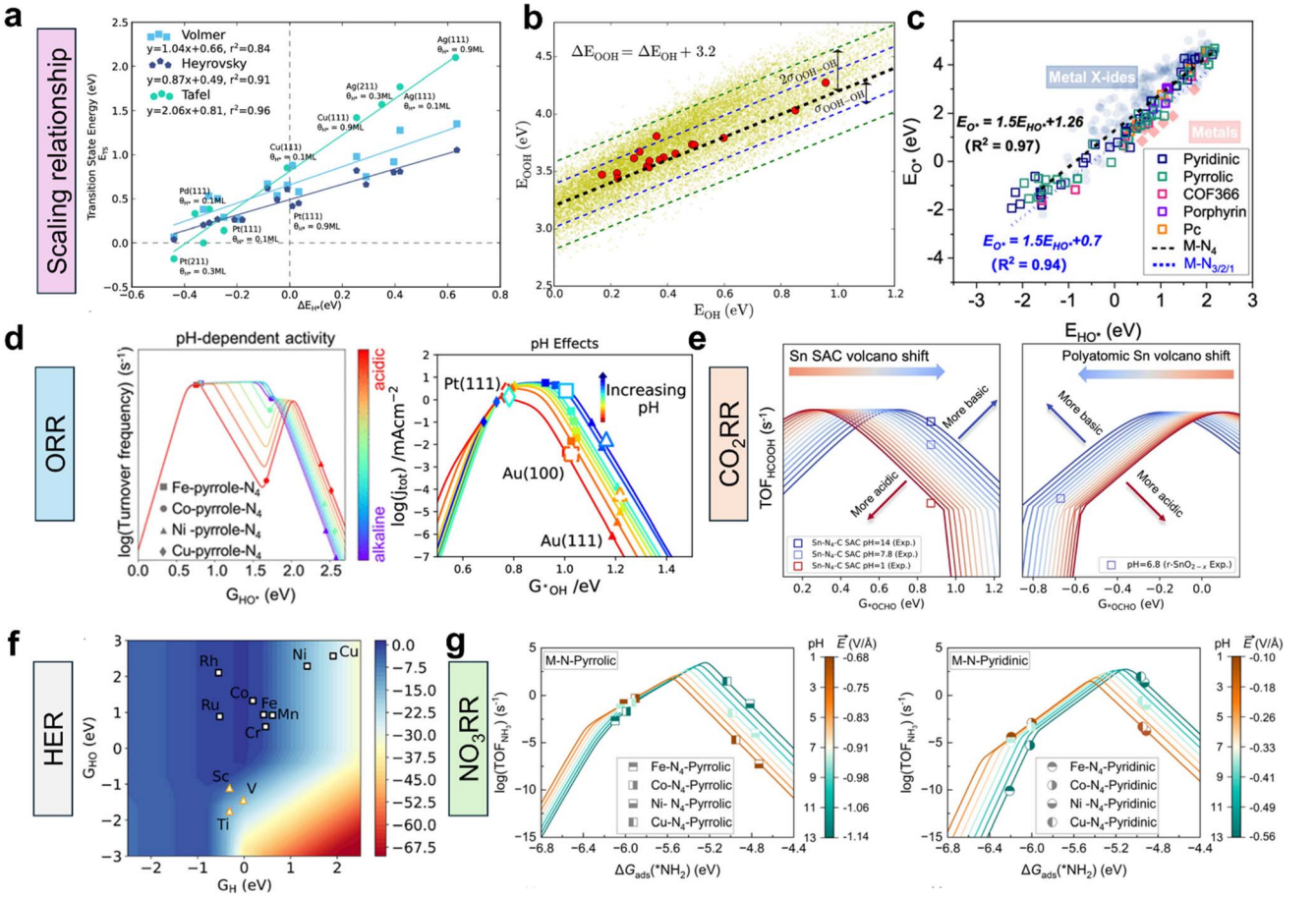

Fig. 5 (a) Scaling relations of the charge extrapolated Volmer, Heyrovsky, and Tafel transition state energies *vs.* H* binding energy. Reproduced with permission.[69] Copyright 2020, American Chemical Society. (b) Plot shows the adsorption energy of the intermediate HOO* plotted against the adsorption energy of the intermediate HO*. The scaling line (black line) has the equation $\Delta E_{OOH} = \Delta E_{OH} + 3.2$ eV. Reproduced with permission.[82] Copyright 2016, American Chemical Society. (c) E_{HO*} *vs.* E_{O*} scaling relations of M–N–C catalysts, metal, and metal oxides. Reproduced with permission.[21] Copyright 2024, American Chemical Society. (d) pH-dependent ORR volcanos of M–N–C catalysts (left) and metal catalysts (right). Reproduced with permission.[16] Copyright 2020, American Chemical Society. (e) pH-dependent CO_2RR volcanos on Sn–N–C catalysts (left) and polyatomic Sn catalysts (right). Reproduced with permission.[54] Copyright 2024, Wiley-VCH. (f) 2D HER volcano considering RHE-scale surface Pourbaix (the orange triangles represent HER activity poisoned by HO*). Reproduced with permission.[22] Copyright 2025, Wiley-VCH. (g) pH-dependent NO_3RR volcano on pyrrolic M–N–C SACs (left) and pyridinic M–N–C SACs (right). Reproduced with permission.[81] Copyright 2025, American Chemical Society.

- HER: a 2D HER microkinetic volcano plot was established,[22] inspired by the RHE-level surface Pourbaix diagram (Fig. 4g and h), which revealed the HO*/O* poisoning effects on SACs. By integrating the RHE-level surface Pourbaix diagram with the 2D volcano plot that explicitly considers HO* poisoning, the long-standing controversy regarding the HER activity of SACs was effectively resolved (*e.g.*, the case of V-pyrrole-N_4, which has an optimized H adsorption energy but poor experimentally observed activity).

- NO_3RR: Jiang *et al.*[81] established the pH-dependent NO_3RR microkinetic model. Notably, subsequent experimental validation confirms the theoretical predictions under both neutral and alkaline conditions (Fig. 5g). This study provides a comprehensive mechanistic framework for understanding the electrocatalytic activity of M–N–C catalysts in NO_3RR, demonstrating that the classical thermodynamic limiting-potential model inadequately captures the rate-determining step and activity trends, especially for M–N–pyrrolic and M–N–pyridinic catalysts. Especially, by integrating microkinetic modelling with electric field effect simulations, the results show that the key elementary steps (such as $*NO_3 \rightarrow *NO_3H$ and $*NO_2 \rightarrow *NO_2H$) should be explicitly considered rather than being dismissed or treated as simultaneous processes.

Notably, in most of the above studies, the catalysts are structurally well-defined and thoroughly characterized, which not only enhances the reliability of the experimental data but also effectively reduces the discrepancies between theoretical calculations and experimental results. The theoretically predicted activity and pH dependence showed good agreement with experimental results, with current densities simulated at the mA level. This provides confidence in elucidating the reaction mechanism. Furthermore, changes in reaction mechanisms can affect the shape of volcanic diagrams. This strategy

offers a promising new approach for accurately capturing the influence of pH in electrochemical systems.

5. Summary and outlook

Understanding the pH dependence of electrocatalytic reactions is essential for the rational design of efficient and durable catalysts, particularly for sustainable processes such as HER, ORR, and CO_2RR, *etc.* In this perspective, we have summarized the major theoretical models developed to capture pH effects, including the conventional CHE model,[83] electric field related model (RHE-level surface Pourbaix diagram and pH-dependent volcano),[1,10,16] and PZCs at explicit/implicit solvation.[67] These frameworks provide valuable insights into the modulation of interfacial properties, such as adsorption energies, reaction barriers, and realistic surface state, under varying pH conditions. To capture the pH-dependent mechanism and activity changes, recent developments, such as microkinetic modeling coupled with electric field, represent promising directions to improve theoretical accuracy and efficiency. Looking forward, a multiscale and dynamic modeling approach that integrates interfacial thermodynamics, kinetics, and solvation effect is urgently needed to fully capture pH-dependent catalytic behavior. In particular: (1) realistic surface states, including dynamic reconstruction, coverage effects and electrode structure, should be considered under operando-relevant pH. Correspondingly, during electrochemical reactions, these dynamic changes also correspond to alterations in PZC and EF effects. This poses a challenge in integrating the EF model with the molecular dynamics simulations. (2) pH not only affects the electric field at the electrode interface and the adsorption of reactants but also significantly alters the solvation structure of solvent molecules, especially the hydrogen-bond network among water molecules, which may lead to theoretical solvation correction change. (3) Machine learning potentials trained on accurate DFT data may help reduce computational cost while preserving fidelity in modeling pH-sensitive interfaces,[80] which would be particularly important to more accurately consider the pH effects, *e.g.*, by including explicit solvation models at various pH conditions. (4) Experiment-theory synergy, such as validating models with pH-dependent Tafel slopes or *in situ* characterizations (*e.g.*, SECCM), will be crucial for model credibility. Ultimately, unraveling the intricate role of pH at the atomic scale not only deepens our fundamental understanding of electrocatalysis but also opens new pathways for designing pH-tolerant or pH-switchable catalysts tailored for a broad range of applications in energy conversion and chemical synthesis.

Conflicts of interest

There are no conflicts to declare.

Data availability

No primary research results, software or code have been included and no new data were generated or analysed as part of this perspective.

Acknowledgements

The authors acknowledge the JSPS KAKENHI (No. JP25K01737, JP24K23068, JP25K17991, JP23K13703, and JP24K17729). S. Y. acknowledges the Japan Science and Technology Agency under the Pioneering Research Initiated by the Next Generation grant (No. JPMJSP2114). A. K. acknowledges JST-PRESTO (No. JPMJPR2274) and JST-MIRAI (No. JPMJMI22I5).

References

1 H. Li, S. Kelly, D. Guevarra, Z. Wang, Y. Wang, J. A. Haber, M. Anand, G. T. K. K. Gunasooriya, C. S. Abraham, S. Vijay, J. M. Gregoire and J. K. Nørskov, Analysis of the limitations in the oxygen reduction activity of transition metal oxide surfaces, *Nat. Catal.*, 2021, **4**(6), 463–468.
2 I. T. McCrum and M. T. M. Koper, The role of adsorbed hydroxide in hydrogen evolution reaction kinetics on modified platinum, *Nat. Energy*, 2020, **5**(11), 891–899.
3 S. Nitopi, E. Bertheussen, S. B. Scott, X. Liu, A. K. Engstfeld, S. Horch, B. Seger, I. E. L. Stephens, K. Chan, C. Hahn, J. K. Norskov, T. F. Jaramillo and I. Chorkendorff, Progress and Perspectives of Electrochemical CO_2 Reduction on Copper in Aqueous Electrolyte, *Chem. Rev.*, 2019, **119**(12), 7610–7672.
4 D. Strmcnik, M. Uchimura, C. Wang, R. Subbaraman, N. Danilovic, D. van der Vliet, A. P. Paulikas, V. R. Stamenkovic and N. M. Markovic, Improving the hydrogen oxidation reaction rate by promotion of hydroxyl adsorption, *Nat. Chem.*, 2013, **5**(4), 300–306.
5 J. Choi, B. H. R. Suryanto, D. Wang, H. L. Du, R. Y. Hodgetts, F. M. F. Vallana, D. R. MacFarlane and A. N. Simonov, Identification and elimination of false positives in electrochemical nitrogen reduction studies, *Nat. Commun.*, 2020, **11**(1), 5546.
6 F. Sun, Q. Tang and D.-e. Jiang, Theoretical Advances in Understanding and Designing the Active Sites for Hydrogen Evolution Reaction, *ACS Catal.*, 2022, **12**(14), 8404–8433.
7 N. Govindarajan, A. Xu and K. Chan, How pH affects electrochemical processes, *Science*, 2022, **375**(6579), 379–380.
8 J. K. Norskov, J. Rossmeisl, A. Logadottir, L. Lindqvist, J. R. Kitchin, T. Bligaard and H. Jonsson, Origin of the Overpotential for Oxygen Reduction at a Fuel-Cell Cathode, *J. Phys. Chem. B*, 2004, **108**(46), 17886–17892.
9 L. Liu, Y. Liu and C. Liu, Enhancing the Understanding of Hydrogen Evolution and Oxidation Reactions on Pt(111) through Ab Initio Simulation of Electrode/Electrolyte Kinetics, *J. Am. Chem. Soc.*, 2020, **142**(11), 4985–4989.
10 H. Liu, D. Zhang, Y. Wang and H. Li, Reversible Hydrogen Electrode (RHE) Scale Dependent Surface Pourbaix Diagram at Different pH, *Langmuir*, 2024, **40**(14), 7632–7638.
11 N. Mahmood, Y. Yao, J. W. Zhang, L. Pan, X. Zhang and J. J. Zou, Electrocatalysts for Hydrogen Evolution in Alkaline Electrolytes: Mechanisms, Challenges, and Prospective Solutions, *Adv. Sci.*, 2018, **5**(2), 1700464.

12 K. Chan and J. K. Norskov, Electrochemical Barriers Made Simple, *J. Phys. Chem. Lett.*, 2015, **6**(14), 2663–2668.
13 K. Chan and J. K. Norskov, Potential Dependence of Electrochemical Barriers from ab Initio Calculations, *J. Phys. Chem. Lett.*, 2016, **7**(9), 1686–1690.
14 T. Liu, Y. Wang and Y. Li, How pH Affects the Oxygen Reduction Reactivity of Fe–N–C Materials, *ACS Catal.*, 2023, **13**(3), 1717–1725.
15 D. M. Patel, A. Tripathi, V. K. Ocampo-Restrepo and G. Kastlunger, Electrocatalysis beyond the reversible hydrogen electrode, *Curr. Opin. Electrochem.*, 2025, **49**, 101611.
16 S. R. Kelly, C. Kirk, K. Chan and J. K. Nørskov, Electric Field Effects in Oxygen Reduction Kinetics: Rationalizing pH Dependence at the Pt(111), Au(111), and Au(100) Electrodes, *J. Phys. Chem. C*, 2020, **124**(27), 14581–14591.
17 P. S. Lamoureux, A. R. Singh and K. Chan, pH Effects on Hydrogen Evolution and Oxidation over Pt(111): Insights from First-Principles, *ACS Catal.*, 2019, **9**(7), 6194–6201.
18 Y. Chen, X. Zhou, X. Liu, Z. Tang, L. Wang and Q. Tang, Understanding the Role of Potential and Cation Effect on Electrocatalytic CO_2 Reduction in All-Alkynyl-Protected Ag_{15} Nanoclusters, *J. Am. Chem. Soc.*, 2025, **147**(3), 2699–2713.
19 P. Li, Y. L. Jiang, Y. Men, Y. Z. Jiao and S. Chen, Kinetic cation effect in alkaline hydrogen electrocatalysis and double layer proton transfer, *Nat. Commun.*, 2025, **16**(1), 1844.
20 S. J. Qian, H. Cao, X. M. Lv, J. Li and Y. G. Wang, Elucidating the Activity of Electrochemical Nitrate Reduction: High-Valent Anionic Intermediates as Kinetic Gatekeepers, *J. Am. Chem. Soc.*, 2025, **147**(24), 21032–21040.
21 D. Zhang, Z. Wang, F. Liu, P. Yi, L. Peng, Y. Chen, L. Wei and H. Li, Unraveling the pH-Dependent Oxygen Reduction Performance on Single-Atom Catalysts: From Single- to Dual-Sabatier Optima, *J. Am. Chem. Soc.*, 2024, **146**(5), 3210–3219.
22 S. Ye, F. Liu, F. She, J. Chen, D. Zhang, A. Kumatani, H. Shiku, L. Wei and H. Li, Hydrogen Binding Energy Is Insufficient for Describing Hydrogen Evolution on Single-Atom Catalysts, *Angew. Chem., Int. Ed.*, 2025, **64**(23), e202425402.
23 L. Cao, Q. Luo, J. Chen, L. Wang, Y. Lin, H. Wang, X. Liu, X. Shen, W. Zhang, W. Liu, Z. Qi, Z. Jiang, J. Yang and T. Yao, Dynamic oxygen adsorption on single-atomic Ruthenium catalyst with high performance for acidic oxygen evolution reaction, *Nat. Commun.*, 2019, **10**(1), 4849.
24 A. E. Russell, Electrocatalysis: theory and experiment at the interface, *Phys. Chem. Chem. Phys.*, 2008, **10**(25), 3607–3608.
25 H. Liu, X. Jia, A. Cao, L. Wei, C. D'Agostino and H. Li, The surface states of transition metal X-ides under electrocatalytic conditions, *J. Chem. Phys.*, 2023, **158**(12), 124705.
26 Y. Furuya, T. Mashio, A. Ohma, M. Tian, F. Kaveh, D. Beauchemin and G. Jerkiewicz, Influence of Electrolyte Composition and pH on Platinum Electrochemical and/or Chemical Dissolution in Aqueous Acidic Media, *ACS Catal.*, 2015, **5**(4), 2605–2614.
27 K. A. Stoerzinger, M. Favaro, P. N. Ross, J. Yano, Z. Liu, Z. Hussain and E. J. Crumlin, Probing the Surface of Platinum during the Hydrogen Evolution Reaction in Alkaline Electrolyte, *J. Phys. Chem. B*, 2018, **122**(2), 864–870.
28 I. Matanović, F. H. Garzon and N. J. Henson, Theoretical Study of Electrochemical Processes on Pt–Ni Alloys, *J. Phys. Chem. C*, 2011, **115**(21), 10640–10650.
29 J. Rossmeisl, J. K. Norskov, C. D. Taylor, M. J. Janik and M. Neurock, Calculated phase diagrams for the electrochemical oxidation and reduction of water over Pt(111), *J. Phys. Chem. B*, 2006, **110**(43), 21833–21839.
30 H. Li, C. S. Abraham, M. Anand, A. Cao and J. K. Norskov, Opportunities and Challenges in Electrolytic Propylene Epoxidation, *J. Phys. Chem. Lett.*, 2022, **13**(9), 2057–2063.
31 H. Li, A. Cao and J. K. Nørskov, Understanding Trends in Ethylene Epoxidation on Group IB Metals, *ACS Catal.*, 2021, **11**(19), 12052–12057.
32 W. G. Cui, F. Gao, G. Na, X. Wang, Z. Li, Y. Yang, Z. Niu, Y. Qu, D. Wang and H. Pan, Insights into the pH effect on hydrogen electrocatalysis, *Chem. Soc. Rev.*, 2024, **53**(20), 10253–10311.
33 L. Zhao, Y. Zhang, Z. Zhao, Q. H. Zhang, L. B. Huang, L. Gu, G. Lu, J. S. Hu and L. J. Wan, Steering elementary steps towards efficient alkaline hydrogen evolution via size-dependent Ni/NiO nanoscale heterosurfaces, *Natl. Sci. Rev.*, 2020, **7**(1), 27–36.
34 Y. Zhu, L. Li, H. Cheng and J. Ma, Alkaline Hydrogen Evolution Reaction Electrocatalysts for Anion Exchange Membrane Water Electrolyzers: Progress and Perspective, *JACS Au*, 2024, **4**(12), 4639–4654.
35 Y. Yuan, J. Li, Y. Zhu, Y. Qiao, Z. Kang, Z. Wang, X. Tian, H. Huang and W. Lai, Water in Electrocatalysis, *Angew. Chem., Int. Ed.*, 2025, **64**(18), e202425590.
36 V. H. Do and J. M. Lee, Transforming Adsorbate Surface Dynamics in Aqueous Electrocatalysis: Pathways to Unconstrained Performance, *Adv. Mater.*, 2025, **37**(10), e2417516.
37 Z. Zhou, Z. Pei, L. Wei, S. Zhao, X. Jian and Y. Chen, Electrocatalytic hydrogen evolution under neutral pH conditions: current understandings, recent advances, and future prospects, *Energy Environ. Sci.*, 2020, **13**(10), 3185–3206.
38 H. Liu, D. Zhang, S. M. Holmes, C. D'Agostino and H. Li, Origin of the superior oxygen reduction activity of zirconium nitride in alkaline media, *Chem. Sci.*, 2023, **14**(34), 9000–9009.
39 T. Wang, Z. Guo, H. Oka, A. Kumatani, C. Liu and H. Li, Origin of electrocatalytic nitrogen reduction activity over transition metal disulfides: critical role of in situ generation of S vacancy, *J. Mater. Chem. A*, 2024, **12**(14), 8438–8446.
40 F. J. Sarabia, P. Sebastian-Pascual, M. T. M. Koper, V. Climent and J. M. Feliu, Effect of the Interfacial Water Structure on the Hydrogen Evolution Reaction on Pt(111) Modified with Different Nickel Hydroxide Coverages in Alkaline Media, *ACS Appl. Mater. Interfaces*, 2019, **11**(1), 613–623.

41 J. Bender, R. Sanspeur, N. B. Ponce, A. Valles, A. Uvodich, D. Milliron, J. Kitchin and J. Resasco, *ChemRxiv*, 2025, preprint, DOI: 10.26434/chemrxiv-2025-qg2sr.
42 A. Tripathi, V. K. Ocampo-Restrepo, J. Nørskov and G. Kastlunger, Field effects explain the unintuitive potential response of electrochemical oxygen evolution in acid, *RSC Sustainability*, 2025, **3**(6), 2659–2668.
43 Y. Yokoyama, K. Miyazaki, Y. Miyahara, T. Fukutsuka and T. Abe, In Situ Measurement of Local pH at Working Electrodes in Neutral pH Solutions by the Rotating Ring-Disk Electrode Technique, *ChemElectroChem*, 2019, **6**(18), 4750–4756.
44 B. Huang, R. R. Rao, S. You, K. H. Myint, Y. Song, Y. Wang, W. Ding, L. Giordano, Y. Zhang, T. Wang, S. Muy, Y. Katayama, J. C. Grossman, A. P. Willard, K. Xu, Y. Jiang and Y. Shao-Horn, Cation- and pH-Dependent Hydrogen Evolution and Oxidation Reaction Kinetics, *JACS Au*, 2021, **1**(10), 1674–1687.
45 Y. Takahashi, Y. Kobayashi, Z. Wang, Y. Ito, M. Ota, H. Ida, A. Kumatani, K. Miyazawa, T. Fujita, H. Shiku, Y. E. Korchev, Y. Miyata, T. Fukuma, M. Chen and T. Matsue, High-Resolution Electrochemical Mapping of the Hydrogen Evolution Reaction on Transition-Metal Dichalcogenide Nanosheets, *Angew. Chem., Int. Ed.*, 2020, **59**(9), 3601–3608.
46 B. Sarkar, D. Das and K. K. Nanda, pH-dependent hydrogen evolution using spatially confined ruthenium on hollow N-doped carbon nanocages as a Mott–Schottky catalyst, *J. Mater. Chem. A*, 2021, **9**(24), 13958–13966.
47 X. Jia, Z. Zhou, F. Liu, T. Wang, Y. Wang, D. Zhang, H. Liu, Y. Wang, S. Ye, K. Amezawa, L. Wei and H. Li, Closed-Loop Framework for Discovering Stable and Low-Cost Bifunctional Metal Oxide Catalysts for Efficient Electrocatalytic Water Splitting in Acid, *J. Am. Chem. Soc.*, 2025, **148**(26), 22642–22654.
48 K. T. Winther, M. J. Hoffmann, J. R. Boes, O. Mamun, M. Bajdich and T. Bligaard, Catalysis-Hub.org, an open electronic structure database for surface reactions, *Sci. Data*, 2019, **6**(1), 75.
49 D. Zhang and H. Li, Digital Catalysis Platform (DigCat): A Gateway to Big Data and AI-Powered Innovations in Catalysis, *ChemRxiv*, 2024, preprint, DOI: 10.26434/chemrxiv-2024-9lpb9.
50 X. Jia, T. Wang, D. Zhang, X. Wang, H. Liu, L. Zhang and H. Li, Advancing electrocatalyst discovery through the lens of data science: State of the art and perspectives, *J. Catal.*, 2025, **447**, 116162.
51 D. Zhang, F. She, J. Chen, L. Wei and H. Li, Why Do Weak-Binding M-N-C Single-Atom Catalysts Possess Anomalously High Oxygen Reduction Activity?, *J. Am. Chem. Soc.*, 2025, **147**(7), 6076–6086.
52 C. Liu, Z. Yu, F. She, J. Chen, F. Liu, J. Qu, J. M. Cairney, C. Wu, K. Liu, W. Yang, H. Zheng, Y. Chen, H. Li and L. Wei, Heterogeneous molecular Co–N–C catalysts for efficient electrochemical H_2O_2 synthesis, *Energy Environ. Sci.*, 2023, **16**(2), 446–459.
53 H. T. Chung, D. A. Cullen, D. Higgins, B. T. Sneed, E. F. Holby, K. L. More and P. Zelenay, Direct atomic-level insight into the active sites of a high-performance PGM-free ORR catalyst, *Science*, 2017, **357**(6350), 479–484.
54 Y. Wang, D. Zhang, B. Sun, X. Jia, L. Zhang, H. Cheng, J. Fan and H. Li, Divergent Activity Shifts of Tin-Based Catalysts for Electrochemical CO_2 Reduction: pH-Dependent Behavior of Single-Atom Versus Polyatomic Structures, *Angew. Chem., Int. Ed.*, 2025, **64**(8), e202418228.
55 Z. Guo, Y. Yu, C. Li, E. C. Dos Santos, T. Wang, H. Li, J. Xu, C. Liu and H. Li, Deciphering Structure-Activity Relationship Towards CO_2 Electroreduction over SnO_2 by A Standard Research Paradigm, *Angew. Chem., Int. Ed.*, 2024, **63**(12), e202319913.
56 L. Li, A. Ozden, S. Guo, A. d. A. F. P. Garci, C. Wang, M. Zhang, J. Zhang, H. Jiang, W. Wang, H. Dong, D. Sinton, E. H. Sargent and M. Zhong, Stable, active CO_2 reduction to formate via redox-modulated stabilization of active sites, *Nat. Commun.*, 2021, **12**(1), 5223.
57 J. B. Mitchell, M. Shen, L. Twight and S. W. Boettcher, Hydrogen-evolution-reaction kinetics pH dependence: is it covered?, *Chem Catal.*, 2022, **2**(2), 236–238.
58 Y. Zhu, M. Klingenhof, C. Gao, T. Koketsu, G. Weiser, Y. Pi, S. Liu, L. Sui, J. Hou, J. Li, H. Jiang, L. Xu, W. H. Huang, C. W. Pao, M. Yang, Z. Hu, P. Strasser and J. Ma, Facilitating alkaline hydrogen evolution reaction on the hetero-interfaced Ru/RuO_2 through Pt single atoms doping, *Nat. Commun.*, 2024, **15**(1), 1447.
59 K. L. Zhou, Z. Wang, C. B. Han, X. Ke, C. Wang, Y. Jin, Q. Zhang, J. Liu, H. Wang and H. Yan, Platinum single-atom catalyst coupled with transition metal/metal oxide heterostructure for accelerating alkaline hydrogen evolution reaction, *Nat. Commun.*, 2021, **12**(1), 3783.
60 H. Li, Z. Jiang, Y. Yuan, Y. Tang, J. Zao, W. Zhang, P. Han, X. Zhang, B. Chen and Y. Liang, Multiscale engineering of molecular electrocatalysts for the rapid hydrogen evolution reaction, *Nano Res.*, 2024, **17**(7), 6026–6031.
61 S. R. Kelly, H. H. Heenen, N. Govindarajan, K. Chan and J. K. Nørskov, OH Binding Energy as a Universal Descriptor of the Potential of Zero Charge on Transition Metal Surfaces, *J. Phys. Chem. C*, 2022, **126**(12), 5521–5528.
62 M. Kim, E. B. Tetteh, O. A. Krysiak, A. Savan, B. Xiao, T. H. Piotrowiak, C. Andronescu, A. Ludwig, T. Dong Chung and W. Schuhmann, Acidic Hydrogen Evolution Electrocatalysis at High-Entropy Alloys Correlates with its Composition-Dependent Potential of Zero Charge, *Angew. Chem., Int. Ed.*, 2023, **62**(39), e202310069.
63 H. Jin, M. Ha, M. G. Kim, J. H. Lee and K. S. Kim, Engineering Pt Coordination Environment with Atomically Dispersed Transition Metal Sites Toward Superior Hydrogen Evolution, *Adv. Energy Mater.*, 2023, **13**(11), 2204213.
64 H. Cao, Q. Wang, Z. Zhang, H. M. Yan, H. Zhao, H. B. Yang, B. Liu, J. Li and Y. G. Wang, Engineering Single-Atom Electrocatalysts for Enhancing Kinetics of Acidic Volmer Reaction, *J. Am. Chem. Soc.*, 2023, **145**(24), 13038–13047.
65 G. Di Liberto, L. A. Cipriano and G. Pacchioni, Role of Dihydride and Dihydrogen Complexes in Hydrogen

Evolution Reaction on Single-Atom Catalysts, *J. Am. Chem. Soc.*, 2021, **143**(48), 20431–20441.

66 M. D. Hossain, Z. Liu, M. Zhuang, X. Yan, G. L. Xu, C. A. Gadre, A. Tyagi, I. H. Abidi, C. J. Sun, H. Wong, A. Guda, Y. Hao, X. Pan, K. Amine and Z. Luo, Rational Design of Graphene-Supported Single Atom Catalysts for Hydrogen Evolution Reaction, *Adv. Energy Mater.*, 2019, **9**(10), 1803689.

67 D. Zhang and H. Li, The potential of zero charge and solvation effects on single-atom M–N–C catalysts for oxygen electrocatalysis, *J. Mater. Chem. A*, 2024, **12**(23), 13742–13750.

68 H. A. Hansen, V. Viswanathan and J. K. Nørskov, Unifying Kinetic and Thermodynamic Analysis of 2 e^- and 4 e^- Reduction of Oxygen on Metal Surfaces, *J. Phys. Chem. C*, 2014, **118**(13), 6706–6718.

69 M. T. Tang, X. Liu, Y. Ji, J. K. Norskov and K. Chan, Modeling Hydrogen Evolution Reaction Kinetics through Explicit Water–Metal Interfaces, *J. Phys. Chem. C*, 2020, **124**(51), 28083–28092.

70 Z. Wang, M. T. Tang, A. Cao, K. Chan and J. K. Nørskov, Insights into the Hydrogen Evolution Reaction on 2D Transition-Metal Dichalcogenides, *J. Phys. Chem. C*, 2022, **126**(11), 5151–5158.

71 D. Zhang, Y. Hirai, K. Nakamura, K. Ito, Y. Matsuo, K. Ishibashi, Y. Hashimoto, H. Yabu and H. Li, Benchmarking pH-field coupled microkinetic modeling against oxygen reduction in large-scale Fe-azaphthalocyanine catalysts, *Chem. Sci.*, 2024, **15**(14), 5123–5132.

72 A. A. Peterson, Global Optimization of Adsorbate–Surface Structures While Preserving Molecular Identity, *Top. Catal.*, 2013, **57**(1–4), 40–53.

73 J. Zhang, Y. Zhao, C. Chen, Y. C. Huang, C. L. Dong, C. J. Chen, R. S. Liu, C. Wang, K. Yan, Y. Li and G. Wang, Tuning the Coordination Environment in Single-Atom Catalysts to Achieve Highly Efficient Oxygen Reduction Reactions, *J. Am. Chem. Soc.*, 2019, **141**(51), 20118–20126.

74 J. Du, G. Han, W. Zhang, L. Li, Y. Yan, Y. Shi, X. Zhang, L. Geng, Z. Wang, Y. Xiong, G. Yin and C. Du, CoIn dual-atom catalyst for hydrogen peroxide production via oxygen reduction reaction in acid, *Nat. Commun.*, 2023, **14**(1), 4766.

75 J. Li, H. Zeng, X. Dong, Y. Ding, S. Hu, R. Zhang, Y. Dai, P. Cui, Z. Xiao, D. Zhao, L. Zhou, T. Zheng, J. Xiao, J. Zeng and C. Xia, Selective CO_2 electrolysis to CO using isolated antimony alloyed copper, *Nat. Commun.*, 2023, **14**(1), 340.

76 A. J. Medford, C. Shi, M. J. Hoffmann, A. C. Lausche, S. R. Fitzgibbon, T. Bligaard and J. K. Nørskov, CatMAP: A Software Package for Descriptor-Based Microkinetic Mapping of Catalytic Trends, *Catal. Lett.*, 2015, **145**(3), 794–807.

77 A. J. Medford, P. G. Moses, K. W. Jacobsen and A. A. Peterson, A Career in Catalysis: Jens Kehlet Nørskov, *ACS Catal.*, 2022, **12**(15), 9679–9689.

78 A. H. Motagamwala and J. A. Dumesic, Microkinetic Modeling: A Tool for Rational Catalyst Design, *Chem. Rev.*, 2021, **121**(2), 1049–1076.

79 K. D. Jensen, J. Tymoczko, J. Rossmeisl, A. S. Bandarenka, I. Chorkendorff, M. Escudero-Escribano and I. E. L. Stephens, Elucidation of the Oxygen Reduction Volcano in Alkaline Media using a Copper-Platinum(111) Alloy, *Angew. Chem., Int. Ed.*, 2018, **57**(11), 2800–2805.

80 Y. Wang, Z. Wu, Y. Jiang, D. Zhang, Q. Wang, C. Wang, H. Li, X. Jia, J. Fan and H. Li, Bridging Theory and Experiment: Machine Learning Potential-Driven Insights into pH-Dependent CO_2 Reduction on Sn-Based Catalysts, *Adv. Funct. Mater.*, 2025, **35**(36), e06314.

81 Q. Jiang, M. Gu, S. Pei, T. Wang, F. Liu, X. Yang, D. Zhang, Z. Wu, Y. Wang, L. Wei and H. Li, The Key Steps and Distinct Performance Trends of Pyrrolic vs. Pyridinic M-N-C Catalysts in Electrocatalytic Nitrate Reduction, *J. Am. Chem. Soc.*, 2025, **147**(29), 26029–26039.

82 S. Deshpande, J. R. Kitchin and V. Viswanathan, Quantifying Uncertainty in Activity Volcano Relationships for Oxygen Reduction Reaction, *ACS Catal.*, 2016, **6**(8), 5251–5259.

83 J. K. Nørskov, T. Bligaard, A. Logadottir, J. R. Kitchin, J. G. Chen, S. Pandelov and U. Stimming, Trends in the Exchange Current for Hydrogen Evolution, *J. Electrochem. Soc.*, 2005, **152**(3), J23–J26.

